Nonlinear Interferometric Vibrational Imaging

Daniel L. Marks and Stephen A. Boppart*

Beckman Institute for Advanced Science and Technology, Department of Electrical and Computer Engineering, University of Illinois at Urbana-Champaign, 405 North Mathews, Urbana, Illinois 61801, USA

(Received 5 November 2003; published 25 March 2004)

Coherent anti-Stokes Raman scattering (CARS) processes are "coherent," but the phase of the anti-Stokes radiation is lost by most incoherent spectroscopic CARS measurements. We propose a Raman microscopy imaging method called nonlinear interferometric vibrational imaging, which measures Raman spectra by obtaining the temporal anti-Stokes signal through nonlinear interferometry. With a more complete knowledge of the anti-Stokes signal, we show through simulations that a high-resolution Raman spectrum can be obtained of a molecule in a single pulse using broad band radiation. This could be useful for identifying the three-dimensional spatial distribution of molecular species in tissue.

DOI: 10.1103/PhysRevLett.92.123905 PACS numbers: 42.65.Dr, 02.30.Zz, 42.25.Hz, 42.62.Be

Molecular imaging techniques have been developed to provide insight into biological processes. Optical molecular imaging is frequently limited because dyes or markers must be introduced that alter or damage biological tissues. Because it is preferable to use endogenous properties of tissues to identify molecular contents, methods such as infrared and Raman spectroscopy are used. In particular, coherent anti-Stokes Raman scattering (CARS) processes have been successfully integrated with confocal scanning microscopes [1–3] to achieve three-dimensional molecular images of vibrational resonances. However, existing instruments measure only the power of the received anti-Stokes radiation. We propose a new technique, nonlinear interferometric vibrational imaging (NIVI), which utilizes nonlinear interferometry to measure the amplitude and phase of the anti-Stokes light. An experimental demonstration of the principle of this technique has been demonstrated [4]. By utilizing NIVI with a properly designed pulse, a large region of the complex Raman susceptibility can be sampled in a single pulse.

Coherent anti-Stokes Raman scattering processes have only recently been used to probe biological specimens. The appeal of CARS is that it probes the density of molecules with a particular Raman resonance frequency while exposing the specimen to low levels of illumination. A typical CARS process illuminates the specimen with a pump pulse of frequency ω_1, and a Stokes pulse of frequency ω_2, which are separated by the vibrational frequency of interest $\Omega = \omega_1 - \omega_2$. If a molecule with a Raman resonance at frequency Ω is present, an anti-Stokes pulse at frequency $2\omega_1 - \omega_2$ is produced. In CARS microscopy, tightly focused pump and Stokes beams are scanned through the specimen, and the anti-Stokes photon count is measured at each point. This photon count is proportional to the square of the molecular bond density and the magnitude of the Raman susceptibility. Nonlinear interferometry has been used to characterize the magnitude of the stimulated Raman scattering nonlinearity in liquids [5], and also of two CARS signals [6] in gases. In addition, the interference between resonant and nonresonant CARS for phase resolution has been demonstrated [7].

The model of CARS with broad band pulses used here is similar to that described previously [8,9]. We do not assume that the illuminating radiation is narrow band. However, we stipulate that the molecule does not resonantly interact directly with any of the frequencies inside the illumination bandwidth or the generated anti-Stokes bandwidth of the optical signal. The CARS process is composed of two stimulated Raman scattering processes involving four photons that begin and end with the molecule in the ground state. To describe CARS, we denote the electric field incident on the molecule as $\tilde{E}_i(\omega)$. The first process is modeled by Eq. (1), and excites the nonlinear dipole polarization of the resonant transition:

$$P^{(3)}(\Omega) = \chi^{(3)}(\Omega) \int_0^\infty \tilde{E}_i(\omega + \Omega)\tilde{E}_i(\omega)^* \, d\omega \text{ (step 1)}, \quad (1)$$

$$\tilde{E}_o(\omega) = \int_0^\omega \tilde{E}_i(\omega - \Omega)P^{(3)}(\Omega) \, d\Omega \text{ (step 2)}. \quad (2)$$

Each pair of frequencies that is separated by a resonance of the molecule at frequency Ω produces a nonlinear polarization in the molecule. Another way to look at Eq. (1) is that, in the time domain, the molecule has a nonlinear polarization that is driven not by the electric field but by the instantaneous intensity envelope of the signal. In this formulation, we neglect any changes in $\chi^{(3)}$ that depend on the "carrier" envelope frequency on which the beats are imposed. Examples of this are pulses that are modulated periodically in the spectral domain with period Ω [10,11], and interfering two relatively delayed chirped pulses to achieve a beat frequency proportional to time delay [12]. The second step, modeled by Eq. (2), creates anti-Stokes radiation by mixing the incoming radiation field with the polarization in the time domain. While these relations do not constitute a linear relationship between $\tilde{E}_i(\omega)$ and $\tilde{E}_o(\omega)$, there is a linear

dependence of $\tilde{E}_o(\omega)$ on $\chi^{(3)}(\Omega)$ given an input field $\tilde{E}_i(\omega)$. This suggests that, with knowledge of the complex $\tilde{E}_o(\omega)$, one can do linear estimation to find $\chi^{(3)}(\Omega)$. The advantage of NIVI over incoherent detection is that nonlinear interferometry enables the recovery of the complex $\tilde{E}_o(\omega)$.

NIVI takes advantage of the coherent nature of the CARS process to allow the phase-sensitive measurement of the anti-Stokes radiation. Conventional linear interferometry involves splitting a source light beam into two parts, each of which scatters linearly in the field, and which are then recombined and detected. NIVI differs in that a CARS process occurs inside the sample.

NIVI can be implemented with the setup detailed in Fig. 1. We start with a broad band, phase-locked source of light pulses, such as those from a mode-locked laser. Sources that produce such light are ultrabroad band mode-locked Ti-sapphire oscillators [15], and supercontinuum sources [16,17]. Because the source is phase locked, there is a deterministic relationship between phases at various frequencies which is preserved by coherent processes such as CARS. To utilize this determinacy, the source bandwidth is split into higher and lower frequency bands, as shown in Fig. 1 with a dichroic beam splitter. The higher frequency band is a reference signal $\tilde{R}(\omega)$, and corresponds to the anti-Stokes frequencies. The lower frequency band is temporally shaped to stimulate CARS in the sample, a signal we denote by the frequency spectrum $\tilde{E}_i(\omega)$. Some of the illumination signal is converted to anti-Stokes radiation by the sample. Because CARS processes are usually rather weak, we assume that any new anti-Stokes radiation created in the same bandwidth as the illumination is inseparable from the illumination. Therefore we discard all anti-Stokes light inside the illumination bandwidth with a high-pass frequency filter. We denote the remaining unfiltered anti-Stokes light by the spectrum $\tilde{E}_o(\omega)$, with frequencies corresponding to those of the reference signal. We combine the reference signal $\tilde{R}(\omega)$ and the anti-Stokes spectrum $\tilde{E}_o(\omega)$ with a 50:50 beam splitter, and measure the interference component with balanced detection on two photodetectors. The reference pulse is delayed by time Δt to facilitate measuring the temporal cross correlation between the reference and anti-Stokes signals. The difference in the two intensities as a function of delay is $\Delta I(\Delta t) = I_+ - I_- = \int_0^\infty 4\,\mathrm{Re}\{\tilde{E}_o(\omega)\tilde{R}(\omega)^* \exp(i\omega\Delta t)\}\,d\omega$. If we call $\tilde{I}(\omega)$ the Fourier transform of $\Delta I(\Delta t)$ with respect to Δt, we find that $\Delta\tilde{I}(\omega) = 4\,\tilde{E}_o(\omega)\tilde{R}(\omega)^*$. Thus, the measured data retains its linear relationship with respect to the anti-Stokes spectrum $\tilde{E}_o(\omega)$ and therefore to $\chi^{(3)}(\Omega)$.

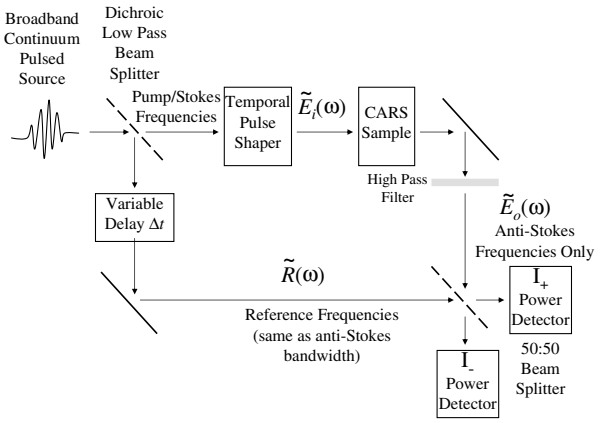

FIG. 1. Schematic of NIVI with a broad band continuum source, using the continuum for the reference pulse. The detection scheme is simplified, and in practice a single-shot detection scheme such as [13,14] could be used.

Besides the ability to find the complex valued $\chi^{(3)}(\Omega)$, interferometry eliminates the need for photon-counting detectors. Another advantage is that interference occurs only when the anti-Stokes light and the reference light arrive at the beam splitter at the same time. Because of this, temporal gating can be used to produce three-dimensional vibrational images in a manner analogous to Optical Coherence Tomography [18–20]. Coherent detection is also far less sensitive to stray light than photon counting. Because of this, NIVI may be more adaptable to various scanning configurations and environments outside the laboratory.

To show that NIVI can measure intervals of the Raman spectrum in a single pulse, a pulse is designed that can stimulate molecules in a broad Raman spectrum. The approach we take creates beats that, instead of being of a constant frequency [12], are themselves chirped. This can be accomplished by combining two chirped pulses with a relative delay, but with different chirp rates. Chirped pulses have the benefit of reducing the nonresonant CARS background. If we have a transform-limited pulsed source of center frequency ω_0 and bandwidth $\Delta\omega$, and we wish to sweep the beat frequency from Ω_L to Ω_H in time T, we can design a pulse $\tilde{E}_i(\omega)$ such that

$$\tilde{E}_i(\omega) = E_0 \cos\!\left(\frac{\pi(\omega-\omega_0)}{\Delta\omega}\right)\left[\left(\frac{1+\kappa}{2}\right)\exp\!\left(\frac{-i(\omega-\omega_0)\tau}{2} - \frac{i(\omega-\omega_0)^2}{2(\alpha+\beta)}\right) + \left(\frac{1-\kappa}{2}\right)\exp\!\left(\frac{i(\omega-\omega_0)\tau}{2} - \frac{i(\omega-\omega_0)^2}{2(\alpha-\beta)}\right)\right] \quad \text{for } \omega_0 - \frac{\Delta\omega}{2} < \omega < \omega_0 + \frac{\Delta\omega}{2},$$

$$\tilde{E}_i(\omega) = 0 \text{ otherwise,} \tag{3}$$

where $\alpha = (2\Delta\omega - \Omega_H - \Omega_L)/2T$, $\beta = (\Omega_H - \Omega_L)/2T$, $\tau = \frac{T}{2}\{[\Omega_H/(\Delta\omega - \Omega_H)] + [\Omega_L/(\Delta\omega - \Omega_L)]\}$. The variable α is the common chirp to both pulses, β is the difference chirp, τ is the time delay between the two pulses, and

κ is the difference in field magnitude between the two pulses. The pulse bandwidth has been apodized with a cosine window because it helps the stability of the inversion. Note that the bandwidth of the source $\Delta\omega$ must exceed Ω_H so that beats can be formed at all Raman frequencies. When creating the pulse, the chirp time T controls the resolution with which one can resolve frequencies in the Raman spectrum. The largest practical T is determined by the dephasing time of the resonances, which in most liquids is on the order of picoseconds.

To demonstrate the feasibility of NIVI, we simulate the illumination of a target molecule with the broad band pulse of Eq. (3) and use the returned signal to estimate the complex susceptibility $\chi^{(3)}(\Omega)$. We show two simulations: one that is able to probe a wide bandwidth of Raman resonances in a single pulse, and the other which is able to distinguish between two nearby resonances. The hypothetical laser source is a mode-locked Ti-sapphire laser that can produce a pulse with a uniform bandwidth from 700–1000 nm, and the setup of Fig. 1. The bandwidth from 800–1000 nm is reserved for stimulating CARS, with the remainder used as the reference signal. For the first simulation, the CARS excitation bandwidth is shaped such that $\Omega_L = 700\ \mathrm{cm}^{-1}$, $\Omega_H = 1300\ \mathrm{cm}^{-1}$, and $T = 5$ ps. To show that the system can reconstruct several simultaneous resonances over the entire bandwidth, we create a hypothetical $\chi^{(3)}(\Omega)$ with several Lorentzian resonances centered at 800, 900, 1000, and 1100 cm^{-1}. These frequencies are in the Raman "fingerprint" region and are useful for practical molecular identification.

The simulation was implemented by sampling the spectra of $\chi^{(3)}(\Omega)$, $\tilde{E}_i(\omega)$, and $\Delta\tilde{I}(\omega)$ at equal intervals from $0\ \mathrm{cm}^{-1}$ to $20\,000\ \mathrm{cm}^{-1}$ in $1.0\ \mathrm{cm}^{-1}$ steps. Equations (1) and (2) form a "forward" CARS linear operator $\mathbf{A}$ computing $\Delta\tilde{I}(\omega)$ from $\chi^{(3)}(\Omega)$ such that $\Delta\tilde{I}(\omega) = \mathbf{A}\chi^{(3)}(\Omega) = \int_0^\omega \chi^{(3)}(\Omega)A(\omega, \Omega)\, d\Omega$, where $A(\omega, \Omega) = \tilde{R}(\omega)^*\tilde{E}_i(\omega - \Omega)\int_0^\infty \tilde{E}_i(\omega' + \Omega)\tilde{E}_i(\omega')^*\, d\omega'$. The Tikhonov-regularized least-squares inversion operator was used to compute the inverse, which is formally denoted by $\mathbf{A}^* = (\mathbf{A}^\dagger\mathbf{W}^\dagger\mathbf{W}\mathbf{A} + \epsilon\mathbf{I})^{-1}\mathbf{A}^\dagger\mathbf{W}^\dagger\mathbf{W}$, where $\mathbf{W}$ was a diagonal weighting operator equal to one inside the measured anti-Stokes bandwidth and zero otherwise. The Tikhonov regularization was included to improve the stability of the inverse, with the constant ϵ chosen to account for the magnitude of noise sources (e.g., photon or thermal) in a realistic experiment. The inverse was computed using the preconditioned conjugate gradient [21] method. Tikhonov regularization adjusts the inverse operator such that unstable features of the estimated spectrum $\chi^{(3)}(\Omega)$ tend to zero.

The left column of Fig. 2 shows the temporal and spectral shapes of the input pulse. Part (a) shows two partially overlapped chirped pulses, producing a beat pattern that stimulates the resonance. Part (b) shows the power spectrum of the input pulse. Part (c) shows the calculated anti-Stokes radiation spectrum. The right column of Fig. 2 shows the original and reconstructed $\chi^{(3)}(\Omega)$. Part (d) is

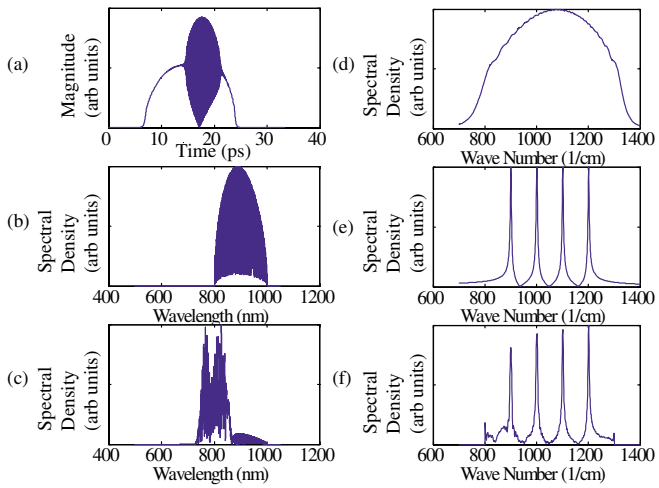

FIG. 2 (color online). NIVI input and output pulses, and the original and reconstructed Raman spectra in first simulation. (a) Temporal shape of amplitude of input pulse. (b) Power spectral density of input pulse. (c) Power spectral density of output pulse. (d) Power spectrum of beat frequencies of input pulse. (e) Magnitude of Raman susceptibility of hypothetical molecule. (f) Magnitude of least-squares reconstructed Raman susceptibility of hypothetical molecule.

the magnitude of the spectrum of the intensity of the original pulse, i.e., the beat frequencies of the pulse. It shows the possible measurable Raman frequencies with this pulse. Part (e) shows the original $\chi^{(3)}(\Omega)$ Raman spectrum magnitude. Finally, part (f) is the Tikhonov-regularized least-squares reconstructed $\chi^{(3)}(\Omega)$ based on only the anti-Stokes frequencies from 700–800 nm. In simulation, all of the spectral lines can be recovered. The minimum discernible separation in Raman frequencies increases as the Raman frequency decreases because the anti-Stokes radiation created by lower frequency resonances overlaps more with the original spectrum.

As a second demonstration with two closely spaced Raman lines, we consider deoxyribonucleic acid (DNA), which would be contained in the nucleus of a cell, and ribonucleic acid (RNA) located throughout the cell. Both macromolecules have PO_2 phosphodiester resonances, but the resonance occurs in DNA at 1094 cm^{-1} and in RNA at 1101 cm^{-1}. To show that a properly designed pulse can recover both resonances distinctly, we create a pulse using Eq. (3) with $\Omega_L = 1070\ \mathrm{cm}^{-1}$, $\Omega_H = 1130\ \mathrm{cm}^{-1}$, and $T = 5$ ps. The results of this simulation are shown in Fig. 3. Figure 3 shows the beat frequency spectrum, and original and reconstructed $\chi^{(3)}(\Omega)$ Raman spectra. While the reconstructed lines are broadened, they are still quite distinct and would be useful for discerning the two molecules.

NIVI is a flexible tool utilizing ultrafast pulses that can measure small or large portions of a Raman spectrum of a molecule in a single pulse. It does so by interferometrically measuring the anti-Stokes radiation from a molecule, stimulated by beats in intensity of an excitation field. From this anti-Stokes field, the complex Raman

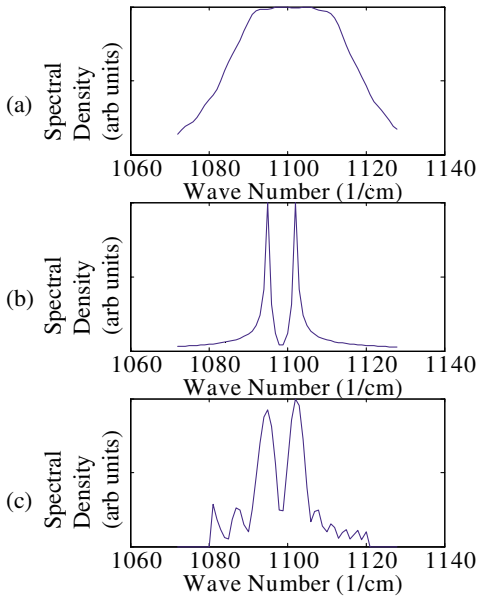

FIG. 3 (color online). Original and reconstructed Raman spectra in second simulation. (a) Power spectrum of beat frequencies of input pulse. (b) Magnitude of Raman susceptibility of hybrid DNA/RNA sample. (c) Magnitude of least-squares reconstructed Raman susceptibility of hybrid DNA/RNA sample.

susceptibility can be estimated. It is especially suited to biological imaging because, while the pulse energy can be large, the peak power can remain small by chirping the pulse. For these reasons, we believe that NIVI can be a general tool for noninvasively probing the molecular content of biological tissues.

We acknowledge the scientific contributions and advice from Jeremy Bredfeldt, Selezion Hambir, Claudio Vinegoni, Martin Gruebele, Dana Dlott, Amy Wiedemann, and Barbara Kitchell from the University of Illinois at Urbana-Champaign. This research was supported in part by the National Aeronautics and Space Administration (NAS2-02057), the National Institutes of Health (National Cancer Institute), and the Beckman Institute for Advanced Science and Technology.

*Also in the Bioengineering Program, the College of Engineering, and the College of Medicine, University of Illinois at Urbana-Champaign, Urbana, IL 61801, USA. Electronic address: boppart@uiuc.edu

[1] M. D. Duncan, J. Reintjes, and T. J. Manuccia, Opt. Lett. **7**, 350 (1982).
[2] E. O. Potma, D. J. Jones, J.-X. Cheng, X. S. Xie, and J. Ye, Opt. Lett. **27**, 1168 (2002).
[3] J.-X. Cheng, L. D. Book, and X. S. Xie, Opt. Lett. **26**, 1341 (2001).
[4] C. Vinegoni, J. S. Bredfeldt, D. L. Marks, and S. A. Boppart, Opt. Express **12**, 331 (2004).
[5] A. Owyoung and P. S. Peercy, J. Appl. Phys. **48**, 674 (1977).
[6] J. W. Hahn and E. S. Lee, J. Opt. Soc. Am. B **12**, 1021 (1995).
[7] D. Oron, N. Dudovich, and Y. Silberberg, Phys. Rev. Lett. **89**, 273001 (2002).
[8] D. Oron, N. Dudovich, D. Yelin, and Y. Silberberg, Phys. Rev. Lett. **88**, 063004 (2002).
[9] D. Oron, N. Dudovich, D. Yelin, and Y. Silberberg, Phys. Rev. A **65**, 043408 (2002).
[10] N. Dudovich, D. Oron, and Y. Silberberg, Nature (London) **418**, 512 (2002).
[11] A. M. Weiner, D. E. Leaird, G. P. Wiederrech, and K. A. Nelson, Science **247**, 1317 (1990).
[12] E. Gershgoren, R. A. Bartels, J. T. Fourkas, R. Tobey, M. M. Murnane, and H. C. Kapteyn, Opt. Lett. **28**, 361 (2003).
[13] K. G. Purchase, D. J. Brady, and K. Wagner, Opt. Lett. **18**, 2129 (1993).
[14] L. Lepetit, G. Cheriaux, and M. Joffre, J. Opt. Soc. Am. B **12**, 2467 (1995).
[15] W. Drexler, U. Morgner, F. X. Kartner, C. Pitris, S. A. Boppart, X. Li, E. P. Ippen, and J. G. Fujimoto, Opt. Lett. **24**, 1221 (1999).
[16] W. J. Wadsworth, A. Ortigosa-Blanch, J. C. Knight, T. A. Birks, T.-P. Martin Man, and P. S. J. Russell, J. Opt. Soc. Am. B **19**, 2148 (2002).
[17] D. L. Marks, A. L. Oldenburg, J. J. Reynolds, and S. A. Boppart, Opt. Lett. **27**, 2010 (2002).
[18] D. Huang *et al.*, Science **254**, 1178 (1991).
[19] S. A. Boppart, B. E. Bouma, C. Pitris, J. F. Southern, M. E. Brezinski, and J. G. Fujimoto, Nature Medicine **4**, 861 (1998).
[20] *Handbook of Optical Coherence Tomography*, edited by B. E. Bouma and G. J. Tearney (Marcel Dekker, New York, 2001).
[21] G. H. Golub and C. F. Van Loan, *Matrix Computations* (Johns Hopkins University Press, Baltimore, MD, 1996).